Supplementary material

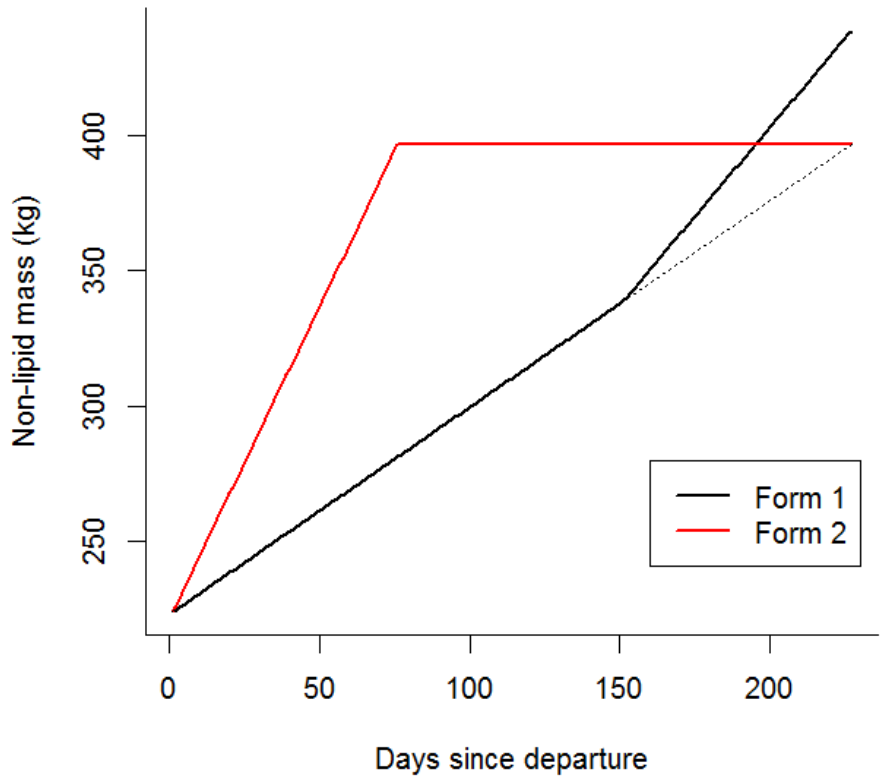

Figure S1. The two functional forms used to represent the variation of a female's non-lipid (lean) mass over the course of a foraging trip. Form 1 assumes a linear increase of female lean mass but accounting for pup mass in the final third of the trip (New et al. 2014), while form 2 assumes the accumulation of female lean mass in the first third of the trip with no influence of pup mass (Schick et al. 2013). The dotted line indicates the increase in female lean mass under form 1 when excluding pup mass.

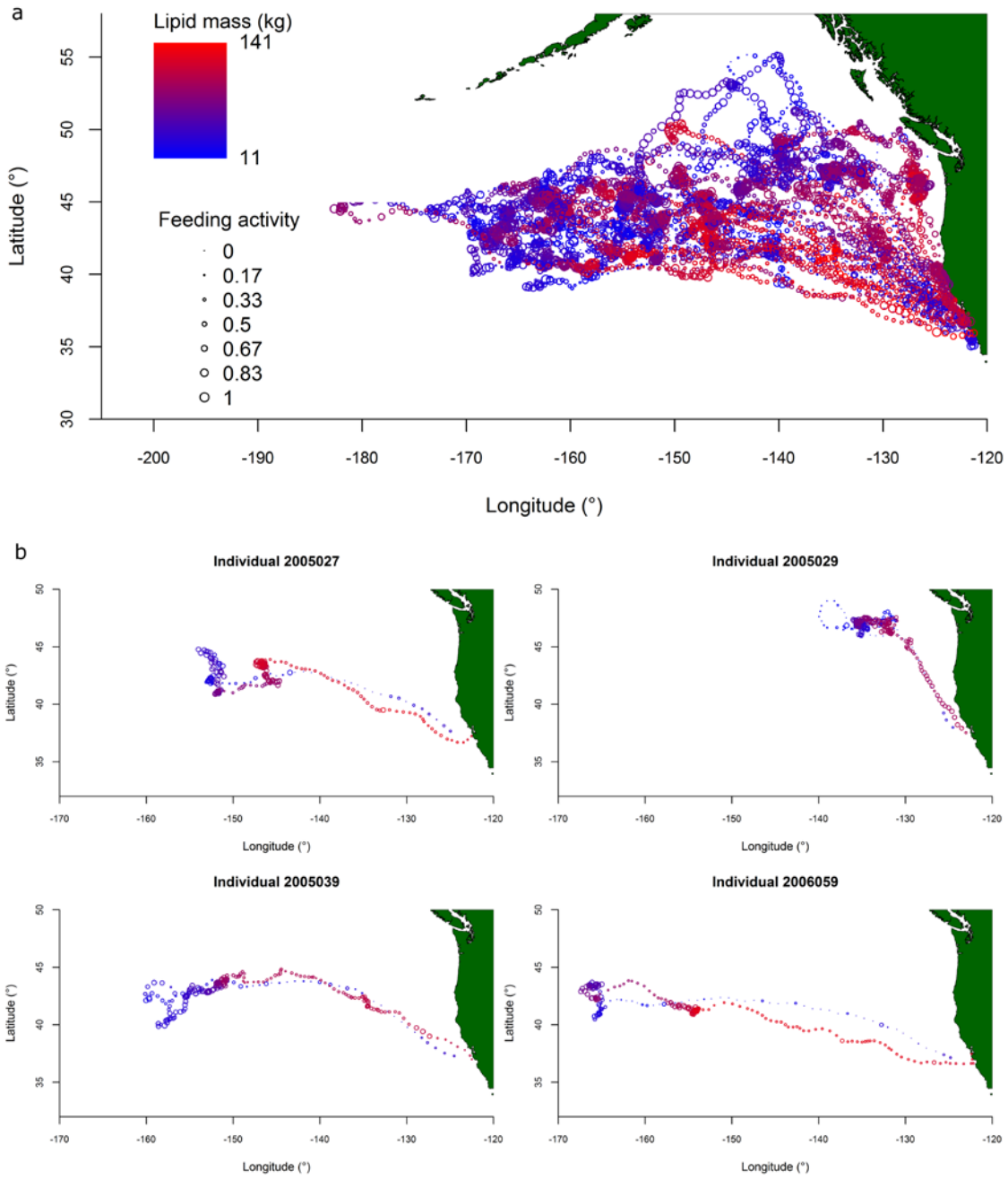

Figure S2. Spatial variation in feeding activity and lipid mass over the course of the foraging trip. The colour gradation indicates the animal's lipid mass, while the size of the dots indicates the corresponding intensity of feeding activity. The coordinates are the daily posterior estimates of individuals' positions. a) All tracks; b) separate tracks of four animals, as an example.

Table S1. Priors and constraints for the parameters of the three model components. Subscript i indicates individual-specific parameters. Acronym N_2 stands for bivariate normal distribution, while ARS stands for area restricted search.

Model component	Parameter	Description	Prior or constraint
Movement	α_1, α_2	Transition probabilities from either movement mode to transiting	*Beta*(1, 1)
	λ_1	Initial probability of being in transiting mode	*Beta*(1, 1)
	λ_2	Initial probability of being in ARS mode	$1 - \lambda_1$
	γ_1	Autocorrelation in direction and speed for transiting mode	*Beta*(2, 1.5)
	g	Deviate to constrain autocorrelation to be lower during ARS	*Beta*(1, 1)
	γ_2	Autocorrelation in direction and speed for ARS mode	$\gamma_1 \cdot g$
	$\log(\psi_i)$	Individual scaling for movement observation model	*Uniform*(-10, 10)
	h_1	Dummy variable for the prior of turning angle in transiting mode	*Beta*(20, 20)
	θ_1	Turning angle in transiting mode	$(2h_1 - 1) \cdot \pi$

	h_2	Dummy variable for the prior of turning angle in ARS mode	*Beta*(10, 10)
	θ_2	Turning angle in ARS mode	$2h_2 \cdot \pi$
	$\boldsymbol{\Sigma_m}$	Covariance matrix of movement process error	*Inverse Wishart*($\begin{pmatrix} 1 & 0 \\ 0 & 1 \end{pmatrix}$, 2)
Feeding	υ_p, υ_n	Effects of being in ARS mode on feeding	*Normal*(1, 1)
	$\boldsymbol{\beta_{i,p}}$	Individual random effects for the dive metrics (positive buoyancy)	$N_2(\mathbf{B_p}, \boldsymbol{\Sigma_p})$
	$B_{1,p}$, $B_{2,p}$	Mean intercept and slope for the random effects (positive buoyancy)	*Normal*(0, 1)
	$\boldsymbol{\Sigma_p}$, $\boldsymbol{\Sigma_n}$	Covariance matrices of individual random effects	*Inverse Wishart*($\begin{pmatrix} 1 & 0 \\ 0 & 1 \end{pmatrix}$, 2)
	$\boldsymbol{\beta_{i,n}}$	Individual random effects for the dive metrics (negative buoyancy)	$N_2(\mathbf{B_n}, \boldsymbol{\Sigma_n})$
	$B_{1,n}$, $B_{2,n}$	Mean intercept and slope for the random effects (negative buoyancy)	*Normal*(0, 1)*
	σ_f^2	Variance of feeding process error	*Inverse Gamma*(e_1, e_2)**
Condition	$\boldsymbol{\zeta_i}$	Individual random effects for condition	$N_2(\mathbf{C}, \boldsymbol{\Sigma_c})$
	C_1, C_2	Mean intercept and slope for the random effects	*Normal*(0, 1)***
	$\boldsymbol{\Sigma_c}$	Covariance matrix for individual random effects	*Inverse Wishart*($\begin{pmatrix} 1 & 0 \\ 0 & 1 \end{pmatrix}$, 2)

	$\boldsymbol{\delta}$	Parameters of condition observation model	$N_2(\mathbf{R}, \boldsymbol{\Sigma}_\mathbf{r})$
	R_1, R_2	Means for the prior of the parameters of condition observation model	0, -1
	$\boldsymbol{\Sigma}_\mathbf{r}$	Covariance matrix for parameters of condition observation model	*Inverse Wishart*($\begin{pmatrix} 1 & 0 \\ 0 & 1 \end{pmatrix}$, 2)
	σ_r^2	Variance of condition observation error	*Inverse Gamma*(S_1, S_2)****
	σ_l^2	Variance of condition process error	*Inverse Gamma* (c_1, c_2)****

*The Gaussian distribution for $B_{2,n}$ was truncated at 0 in order to facilitate convergence by constraining the number of dives per day to have a negative effect on feeding activity (as suggested by the mixed effects models).

**e_1 = 18 and e_2 = 0.05. These values were chosen so that the distribution was centred on 0.003, i.e. the unexplained error in feeding activity was at most 0.05 when feeding activity was 0.5.

***The Gaussian distribution for C_2 was truncated at 0 in order to constrain feeding activity to have a positive effect on lipid mass.

****Following Schick et al. (2013), $S_1 = 10 \cdot T$, where T was the overall sample size, and $S_2 = 4 \cdot (S_1 - 1)$, implying that the variance of drift rate was centered on 1 (before scaling by the number of drift dives). Similarly, $c_1 = T/2$ and $c_2 = c_1 - 1$, meaning that the variance of the lipid mass was centered on 4.

Table S2. Posterior estimates of parameters of interest (median and 95% highest posterior density interval). For each parameter, the table also reports the effective sample size and convergence diagnostics: upper confidence interval (CI) of the Brooks-Gelman-Rubin (BGR) diagnostic and percentage of Monte Carlo error (MCE) to sample standard deviation (SSD).

Parameter	Lower (2.5%)	Median	Upper (97.5%)	Effective sample size	BGR diagnostic (upper CI)	% MCE/SSD
α_1	0.96	0.97	0.98	14540	1.00	0.8
α_2	0.04	0.05	0.07	12807	1.00	0.9
γ_1	0.86	0.87	0.88	16484	1.00	0.8
γ_2	0.00	0.04	0.12	9887	1.00	1.0
θ_1	0.00	0.01	0.02	18122	1.00	0.7
θ_2	2.28	3.23	4.24	17375	1.00	0.8
υ_p	1.20	2.39	3.85	9453	1.00	1.0
υ_n	0.50	1.73	3.24	12306	1.00	0.9
$B_{1,\mathrm{p}}$	-1.18	-0.24	0.67	2703	1.01	1.9
$B_{2,\mathrm{p}}$	-0.44	0.32	1.18	5773	1.01	1.3
$B_{1,\mathrm{n}}$	-1.09	-0.04	0.97	4678	1.01	1.5
$B_{2,\mathrm{n}}$	-3.34	-2.11	-1.23	6933	1.00	1.2
C_1	-1.01	-0.57	-0.26	2287	1.00	2.1
C_2	1.19	1.62	2.15	1411	1.00	2.7
δ_0	-0.56	-0.49	-0.43	462	1.01	4.6
δ_1	2.18	2.46	2.77	551	1.02	4.3
σ_f^2	0.002	0.003	0.005	5234	1.00	1.4
σ_r^2	3.97	4.00	4.03	17618	1.00	0.8
σ_l^2	0.54	0.55	0.57	17516	1.00	0.8

Appendix S1. Mixed effects models to select dive metrics.

The daily median dive metrics that best correlated with the drift rate in the following day were identified using a mixed effects modelling approach, where drift rate in the following day was the response variable, each dive metric was the explanatory variable and seal ID number was used as an individual random effect. Data exploration suggested that the relationship between each dive metric and drift rate varied depending on the sign of the latter. Therefore, separate models were fitted for positive and negative values of the drift rate. The candidate explanatory variables were: daily median ascent rate, daily median descent rate, daily median time spent at the bottom during a dive, total number of dives per day and daily median dive duration. The analysis was carried out using package lme4 in R (Bates et al. 2012) and models were fitted using maximum likelihood. Models were compared using Akaike's Information Criterion (AIC) and results of model selection are reported below. Total number of dives minimised the AIC in the model for negative buoyancy, while median ascent rate was the best explanatory variable when buoyancy was positive.

Dive metric	**AIC**
Negative buoyancy (drift rate < 0)	
Intercept-only	-5722
Ascent rate	-6052
Descent rate	-6588
Bottom time	-6935
Total number of dives	-7084
Dive duration	-6397
Positive buoyancy (drift rate ≥ 0)	
Intercept-only	-5555
Ascent rate	-5623
Descent rate	-5560
Bottom time	-5567
Total number of dives	-5554
Dive duration	-5555

Appendix S2. Argos Location error.

The scale parameters ($\tau_{lat,q}$ and $\tau_{lon,q}$) and degrees of freedom ($\nu_{lat,q}$ and $\nu_{lon,q}$) of the *t*-distributions of the observation errors on each coordinate (latitude and longitude), given location class *q*, were estimated from published data on class-specific Argos location accuracy (Costa et al. 2010). Maximum likelihood estimates and standard errors were obtained using the library MASS (Venables and Ripley 2002) in R, and are summarised below. All estimates are in km. These parameters were then treated as known in the movement component of the model, following Jonsen et al. (2005).

Quality class	**Longitude**		**Latitude**	
	τ_{lon} (SE)	ν_{lon} (SE)	τ_{lat} (SE)	ν_{lat} (SE)
Z	49.826 (16.161)	1.286 (0.544)	13.994 (5.493)	0.941 (0.373)
B	3.679 (0.374)	0.786 (0.070)	2.472 (0.225)	0.975 (0.092)
A	1.827 (0.255)	0.797 (0.097)	1.617 (0.190)	1.021 (0.129)
0	1.730 (0.232)	1.272 (0.211)	1.207 (0.145)	1.641 (0.303)
1	0.767 (0.061)	3.388 (0.764)	0.437 (0.039)	1.976 (0.316)
2	0.528 (0.073)	2.424 (0.713)	0.356 (0.048)	1.821 (0.412)
3	0.269 (0.077)	1.734 (0.792)	0.130 (0.037)	1.460 (0.574)

Appendix S3. Joint likelihood

The joint conditional likelihood (L) of the observations (daily median drift rate, **r**; mean lipid mass at arrival, $\mathbf{m_{Ti}}$; and the matrix, **Y**, of Argos coordinate pairs, **y**) and all latent variables (the matrix, **X**, of true daily locations, **x**; movement mode, **b**; feeding activity, **f**; and lipid mass, **l**) can be expressed as the product of their independent likelihoods (McClintock et al. 2013):

$$
\begin{aligned}
&L(\mathbf{r},\mathbf{Y},\mathbf{X},\mathbf{b},\mathbf{f},\mathbf{l},\mathbf{m}_{\mathbf{T_i}} \mid \boldsymbol{\iota},\mathbf{q},\mathbf{m_1},\boldsymbol{\varphi},\mathbf{s},\mathbf{n},\mathbf{a},\mathbf{D}) = \prod_{i=1}^{I}\Big\{L(l_{i,1} \mid m_{i,1},\varphi_{i,1}) \cdot L(b_{i,1} \mid \boldsymbol{\iota}) \cdot \\
&L(\mathbf{x_{i,1}} \mid \boldsymbol{\iota},\mathbf{y_{1,i,1}},q_{1,i,1}) \cdot L(\mathbf{x_{i,2}} \mid \boldsymbol{\iota},\mathbf{x_{i,1}}) \cdot \prod_{t=2}^{T_i-1}\Big[L(b_{i,t} \mid \boldsymbol{\iota},b_{i,t-1}) \cdot L(\mathbf{x_{i,t+1}} \mid \boldsymbol{\iota},\mathbf{x_{i,t}},\mathbf{x_{i,t-1}},b_{i,t}) \cdot \\
&L(f_{i,t} \mid \boldsymbol{\iota},s_{i,t},n_{i,t},b_{i,t},r_{i,t}) \cdot L(l_{i,t} \mid \boldsymbol{\iota},l_{i,t-1},f_{i,t}) \cdot L(r_{i,t} \mid \boldsymbol{\iota},l_{i,t},a_{i,t},D_{i,t}) \cdot \\
&\prod_{z=1}^{Z_{i,t}} L(\mathbf{y_{z,i,t}} \mid \boldsymbol{\iota},\mathbf{x_{i,t}},\mathbf{x_{i,t-1}},q_{z,i,t})\Big] \cdot L(b_{i,T_i} \mid \boldsymbol{\iota},b_{i,T_i-1}) \cdot L(f_{i,T_i} \mid \boldsymbol{\iota},s_{i,T_i},n_{i,T_i},b_{i,T_i},r_{i,T_i}) \cdot \\
&L(l_{i,T_i} \mid \boldsymbol{\iota},l_{i,T_i-1},f_{i,T_i}) \cdot L(r_{i,T_i} \mid \boldsymbol{\iota},l_{i,T_i},a_{i,T_i},D_{i,T_i}) \cdot L(m_{i,T_i} \mid l_{i,T_i},\varphi_{i,T_i}) \cdot \\
&\prod_{z=1}^{Z_{i,T_i}} L(\mathbf{y_{z,i,T_i}} \mid \boldsymbol{\iota},\mathbf{x_{i,T_i}},\mathbf{x_{i,T_i-1}},q_{z,i,T_i})\Big\}
\end{aligned}
$$

where $\boldsymbol{\iota}$ denotes the set of all model parameters, **q** is the vector of Argos quality class for each observed location, $\mathbf{m_1}$ is the vector of empirical mean lipid mass at departure (t = 1), $\boldsymbol{\varphi}$ is the vector of empirical standard deviation of lipid mass at departure (t = 1) and arrival ($t = T_i$), **a** is the vector of daily lean mass, **D** is the vector of the number of drift dives per day, **n** is the vector of total number of dives per day, **s** is the vector of daily median ascent rate, I is the total number of individuals, T_i is the duration of each individual's trip and $Z_{i,t}$ is the number of Argos locations recorded for each individual on each day of the trip.

Appendix S4. Model code

```
model
{

pi <- 3.141592653589

#Hyperparameters for Wishart priors of covariance matrices
pr.cov[1,1] <- 1
pr.cov[1,2] <- 0
pr.cov[2,1] <- 0
pr.cov[2,2] <- 1

#Priors and constraints for parameters of the movement component
alpha[1] ~ dbeta(1,1)           #transition probability (transit to transit)
alpha[2] ~ dbeta(1,1)           #transition probability (ARS to transit)
lambda[1] ~ dbeta(1,1)          #initial probability of being in transit mode
lambda[2] <- 1 - lambda[1]      #initial probability of being in ARS mode
gamma[1] ~ dbeta(2,1.5)         #autocorrelation parameter - transit mode
g ~ dbeta(1,1)                  #deviate to ensure gamma[2] < gamma[1]
gamma[2] <- gamma[1] * g        #autocorrelation parameter - ARS mode
h[1] ~ dbeta(20,20)             #dummy variable
h[2] ~ dbeta(10,10)             #dummy variable
theta[1] <- (2 * h[1] - 1) * pi #turning angle - transit mode
theta[2] <- 2 * h[2] * pi       #turning angle - ARS mode
iSigma_m[1:2,1:2] ~ dwish(pr.cov[,],2)
Sigma_m[1:2,1:2] <- inverse(iSigma_m[1:2,1:2]) #covariance matrix

#Priors and constraints for parameters of the feeding component
upsilon[1] ~ dnorm(1,1)         #effect of being in ARS mode (when positively buoyant) on feeding
                                 activity
upsilon[2] ~ dnorm(1,1)         #effect of being in ARS mode (when negatively buoyant) on feeding
                                 activity
Bp[1] ~ dnorm(0,1)              #mean intercept (when positively buoyant)
Bp[2] ~ dnorm(0,1)              #mean effect of ascent rate on feeding activity
iSigma_p[1:2,1:2] ~ dwish(pr.cov[,],2)
Sigma_p[1:2,1:2] <- inverse(iSigma_p[1:2,1:2]) #covariance matrix
```

```
Bn[1] ~ dnorm(0,1)              #mean intercept (when negatively buoyant)
Bn[2] ~ dnorm(0,1)T(-100,0)     #mean effect of number of dives on feeding activity
iSigma_n[1:2,1:2] ~ dwish(pr.cov[,],2)
Sigma_n[1:2,1:2] <- inverse(iSigma_n[1:2,1:2]) #covariance matrix
tau_f ~ dgamma(18,0.05)         #process precision
sigma2_f <- 1/tau_f             #process variance

#Priors and constraints for parameters of the condition component
C[1] ~ dnorm(0,1)               #mean intercept
C[2] ~ dnorm(0,1)T(0,100)       #mean effect of feeding activity on lipid gain
iSigma_C[1:2,1:2] ~ dwish(pr.cov[,],2)
Sigma_C[1:2,1:2] <- inverse(iSigma_C[1:2,1:2]) #covariance matrix
c1 <- Xidx[I+1]/2               #hyperparameter for process uncertainty
c2 <- c1-1                      #hyperparameter for process uncertainty
tau_l ~ dgamma(c1,c2)           #process precision
sigma2_l <- 1/tau_l             #process variance

#Priors for condition observation model
R[1] <- 0                       #hyperparameter for bivariate prior
R[2] <- -1                      #hyperparameter for bivariate prior
iSigma_r[1:2,1:2] ~ dwish(pr.cov[,],2)
Sigma_r[1:2,1:2] <- inverse(iSigma_r[1:2,1:2]) #covariance matrix
delta[1:2] ~ dmnorm(R[1:2],iSigma_r[1:2,1:2])  #intercept and effect of buoyancy on drift rate
                                                (correlated)
S1 <- 10*Xidx[I+1]              #hyperparameter for measurement uncertainty
S2 <- 4*(S1-1)                  #hyperparameter for measurement uncertainty
tau_r ~ dgamma(S1,S2)           #measurement precision
sigma2_r <- 1/tau_r             #measurement variance

#Priors for NAs in number of drift dives
for (d in 1:lna.dd){            #cycle through NAs in the data (previously identified)
  D[nas.dd[d]] ~ dnorm(pr.dd[d],1)T(range.dd[1],range.dd[2])
  }
```

```
for(i in 1:I){                  #cycle through I individuals

  #Individual-specific scaling parameter for t-distributed error
  log.psi[i] ~ dunif(-10,10)
  psi[i] <- exp(log.psi[i])

  #Individual-specific parameters for feeding component
  beta_p[i,1:2] ~ dmnorm(Bp[1:2], iSigma_p[1:2,1:2])
  beta_n[i,1:2] ~ dmnorm(Bn[1:2], iSigma_n[1:2,1:2])

  #Individual-specific parameters for condition component
  zeta[i,1:2] ~ dmnorm(C[1:2],iSigma_C[1:2,1:2])

  #Precision of initial and final mass measurements (from empirical standard deviation phi1 at t=1
   and phiT t=Ti)
  tau_m1[i] <- 1/phi1[i]/phi1[i]
  tau_mT[i] <- 1/phiT[i]/phiT[i]

  #Initial lipid mass (from initial mass measurement)
  l[Xidx[i]] ~ dnorm(m[i,1],tau_m1[i])

  #Initial behavioral mode
  b[Xidx[i]] ~ dcat(lambda[])   #1=transit, 2=ARS

  #Initial location
  first.loc[i,1] <- y[Yidx[i],1]
  first.loc[i,2] <- y[Yidx[i],2]
  for(c in 1:2){
    itau2psi[i,c] <- itau2[Xidx[i],c] * psi[i]
    x[Xidx[i],c] ~ dt(first.loc[i,c], itau2psi[i,c], nu[Xidx[i],c])
    }

  #Second location
  x[(Xidx[i]+1),1:2] ~ dmnorm(x[Xidx[i],],iSigma_m[,])     #assume simple random walk to estimate
                                                            2nd regular position
```

```
for(t in (Xidx[i]+1):(Xidx[i+1]-2)){            #cycle through time steps for each individual

  #Movement component
  prob[t,1] <- alpha[b[t-1]]                    #transition probability from previous mode to
                                                 transit mode
  prob[t,2] <- 1 - alpha[b[t-1]]                #transition probability from previous mode to
                                                 ARS mode
  b[t] ~ dcat(prob[t,])                         #behavioural mode (1=transit, 2=ARS)
  Tdx[t,1] <- cos(theta[b[t]]) * (x[t,1] - x[t-1,1]) + sin(theta[b[t]]) * (x[t,2] - x[t-1,2])
  Tdx[t,2] <- -sin(theta[b[t]]) * (x[t,1] - x[t-1,1]) + cos(theta[b[t]]) * (x[t,2] - x[t-1,2])
  x.mn[t,1] <- x[t,1] +  Tdx[t,1] * gamma[b[t]]
  x.mn[t,2] <- x[t,2] +  Tdx[t,2] * gamma[b[t]]
  x[t+1,1:2] ~ dmnorm(x.mn[t,],iSigma_m[,])     #next location (with process error)

  #Feeding component
  logit.f[t] <- indicator[t]*(beta_p[i,1] + upsilon[1]*(b[t]-1) + beta_p[i,2]*s[t]) + (1-
    indicator[t])*(beta_n[i,1]+ upsilon[2]*(b[t]-1) + beta_n[i,2]*n[t]) + epsilon[t]
  epsilon[t] ~ dnorm(0,tau_f)                   #process error
  f[t] <- exp(logit.f[t])/(1 + exp(logit.f[t]))  #feeding activity

  #Condition component
  l.mu[t] <- l[t-1] + zeta[i,1] + zeta[i,2]*f[t]
  l[t] ~ dnorm(l.mu[t],tau_l)                   #lipid mass (with process error)

  #Condition observation model
  r.mu[t] <- delta[1] + delta[2]*l[t]/a[t]      #mean drift rate (as a function of buoyancy)
  sigma2_rD[t] <- sigma2_r/(D[t]+1)             #adjust variance by number of drift dives
  tau_rD[t] <- 1/sigma2_rD[t]
  r[t] ~ dnorm(r.mu[t],tau_rD[t])               #drift rate (observed)
  }

#Final time step:
#Final behavioral mode
fprob[i,1] <- alpha[b[Xidx[i+1]-2]]   #transition probability from previous mode to transit mode
fprob[i,2] <- 1 - fprob[i,1]          #transition probability from previous mode to ARS mode
b[Xidx[i+1]-1] ~ dcat(fprob[i,])
```

```
  #Final feeding activity
  logit.f[Xidx[i+1]-1] <- indicator[Xidx[i+1]-1]*(beta_p[i,1] + upsilon[1]*(b[Xidx[i+1]-1]-1) +
   beta_p[i,2]*s[Xidx[i+1]-1]) + (1-indicator[Xidx[i+1]-1])*(beta_n[i,1] +
   upsilon[2]*(b[Xidx[i+1]-1]-1) + beta_n[i,2]*n[Xidx[i+1]-1]) + epsilon[Xidx[i+1]-1]
  epsilon[Xidx[i+1]-1] ~ dnorm(0,tau_f)
  f[Xidx[i+1]-1] <- exp(logit.f[Xidx[i+1]-1])/(1 + exp(logit.f[Xidx[i+1]-1]))  #feeding activity
  #Final condition
  l.mu[Xidx[i+1]-1] <- l[Xidx[i+1]-2] + zeta[i,1] + zeta[i,2]*f[Xidx[i+1]-1]
  l[Xidx[i+1]-1] ~ dnorm(l.mu[Xidx[i+1]-1],tau_l)                              #lipid mass
  m[i,2] ~ dnorm(l[Xidx[i+1]-1],tau_mT[i])                                     #final mass
                                                                               measurement used
                                                                               as sample of final
                                                                               lipid mass

  #Observation model for final condition
  r.mu[Xidx[i+1]-1] <- (delta[1] + delta[2]*l[Xidx[i+1]-1]/a[Xidx[i+1]-1])     #true drift rate
  sigma2_rD[Xidx[i+1]-1] <- sigma2_r/(D[Xidx[i+1]-1]+1)                        #adjust variance by
                                                                               number of drift
                                                                               dives
  tau_rD[Xidx[i+1]-1] <- 1/sigma2_rD[Xidx[i+1]-1]
  r[Xidx[i+1]-1] ~ dnorm(r.mu[Xidx[i+1]-1],tau_rD[Xidx[i+1]-1])                #observed drift
                                                                               rate

  #Movement observation model
  for(t in (Xidx[i]+1):(Xidx[i+1]-1)){  #cycle through regular time steps
    for(z in idx[t]:(idx[t+1]-1)){      #cycle through observed locations within interval t
      for(c in 1:2){                    #for each coordinate (lon and lat)
        zhat[z,c] <- (1-j[z]) * x[t-1,c] + j[z] * x[t,c] #true location (given position within
                                                          interval)
        itau2psi2[z,c] <- itau2[z,c] * psi[i]
        y[z,c] ~ dt(zhat[z,c],itau2psi2[z,c],nu[z,c])    #observed location
        }
      }
    }
   }
}
```

Table S3. Individual activity budgets as estimated by the movement component of the model.

Individual ID	Transit (%)	Area restricted search (%)	Uncertain (%)
2004020	88	8	4
2004021	81	5	14
2004024	65	19	16
2004029	60	30	10
2004030	54	30	16
2004032	63	18	19
2004035	62	20	18
2005021	61	15	24
2005024	50	45	5
2005027	41	46	13
2005028	21	70	9
2005029	37	47	16
2005031	73	16	11
2005034	56	30	14
2005036	86	11	3
2005039	59	27	14
2005040	66	30	4
2006041	54	36	10
2006044	74	17	9
2006048	66	17	17
2006055	73	19	8
2006057	67	20	13
2006059	58	33	9
2007033	57	32	11
2007034	49	41	10
2007040	53	31	16

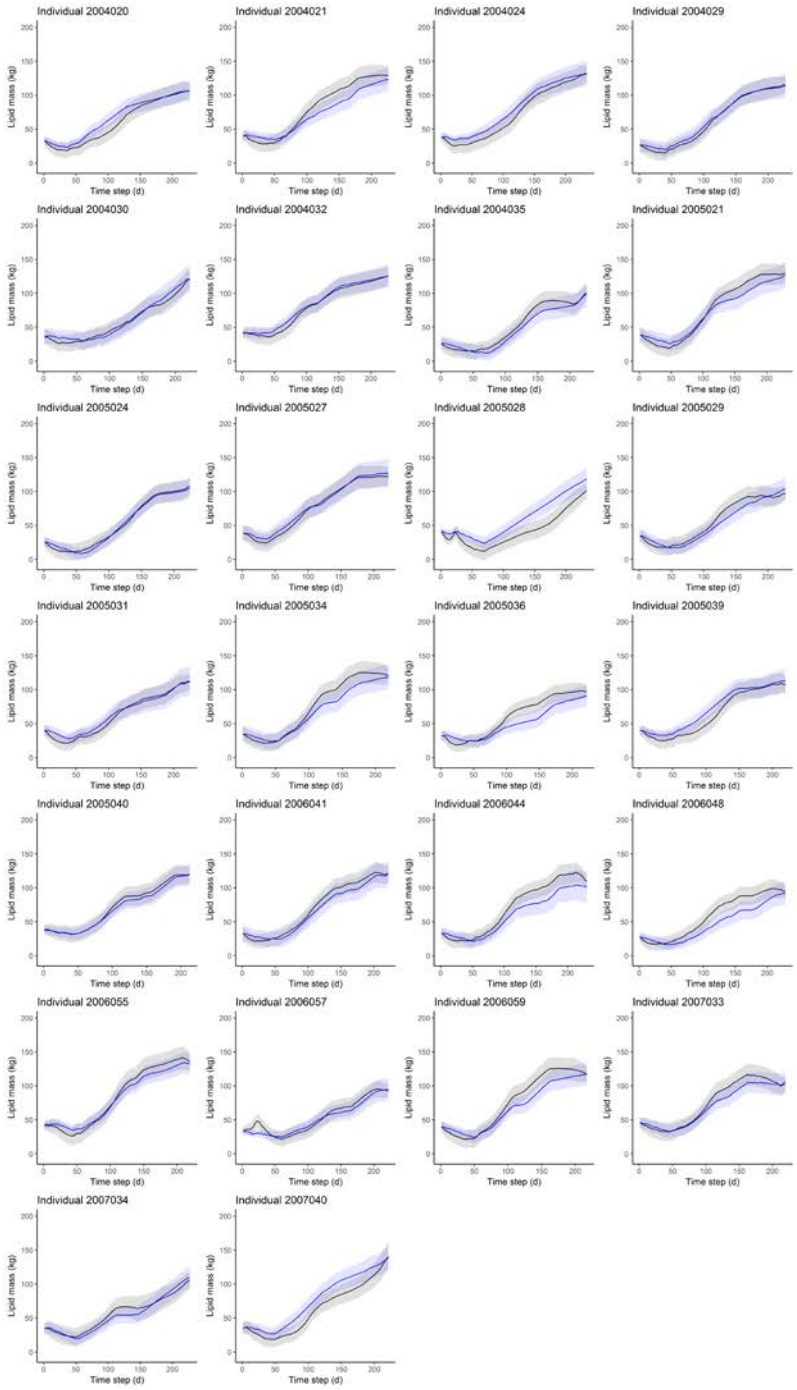

Figure S3. Posterior estimates of the lipid mass (black) overlaid with the time series of lipid masses obtained using the process model only (i.e. calculated from the initial lipid mass and the estimated feeding activity at each time step) (blue). The shaded area represents the uncertainty in the estimates and predictions.

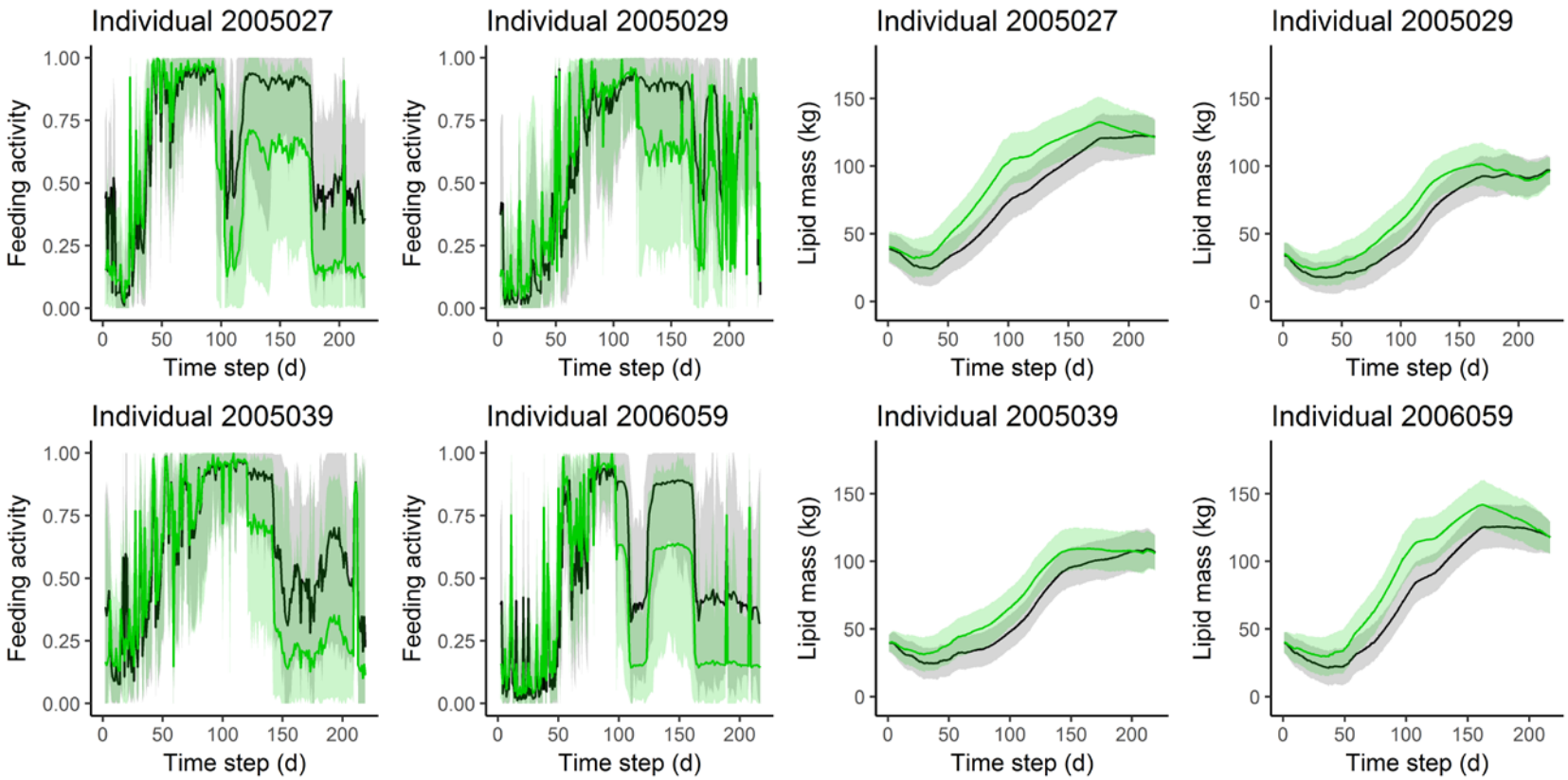

Figure S4. Comparison of the estimated feeding activity (on the left) and variation in lipid mass (on the right) given the two functional forms for the variation of lean mass (in black functional form 1, used in the final model, in green functional form 2) for four individuals. The solid lines represent the median estimates, and the shaded bands the uncertainty around these estimates.

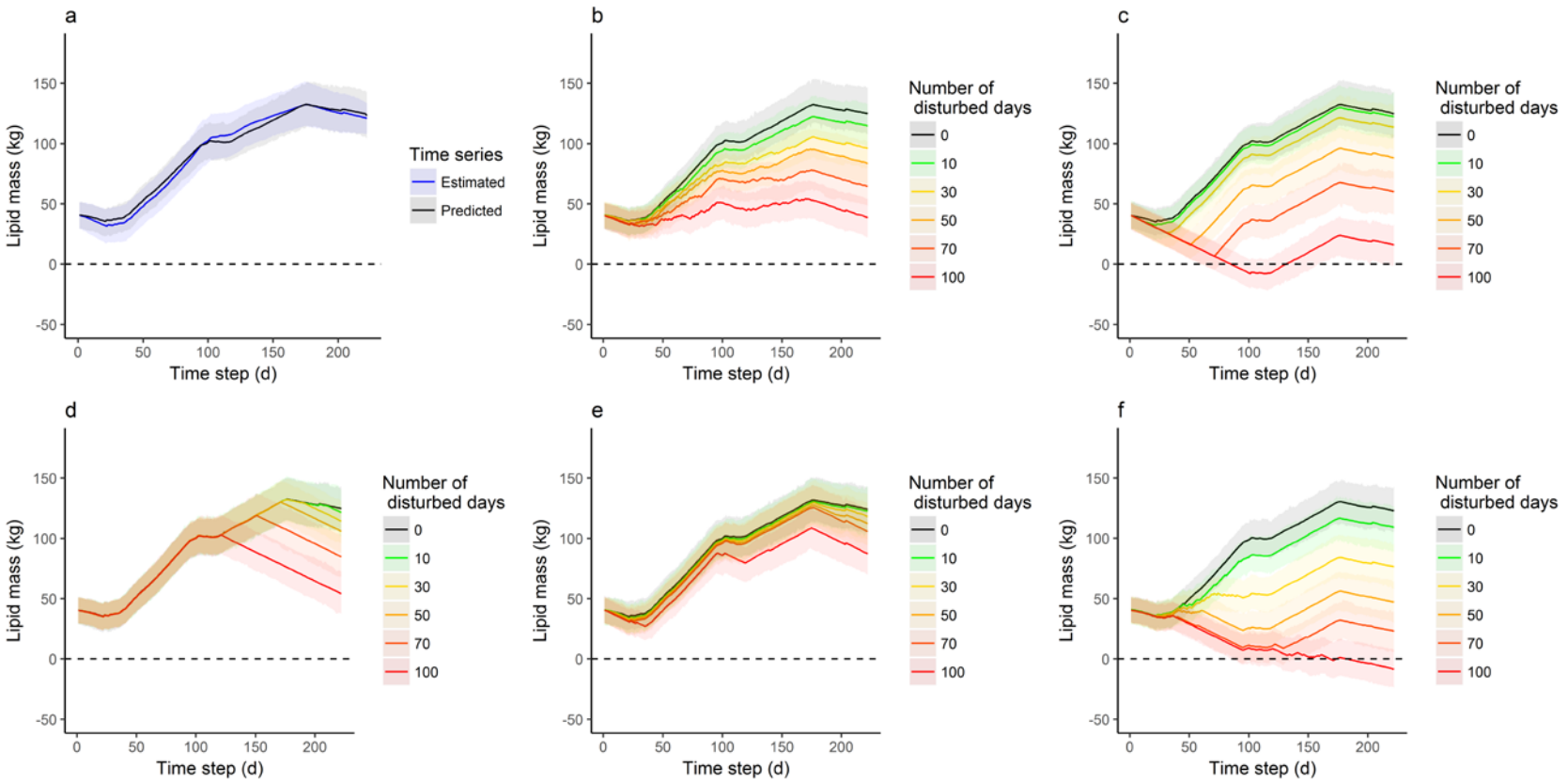

Figure S5. Simulated effects of an increased number of disturbed days on the lipid mass of individual 2005027, given the second functional form for the variation of the lean mass. a) Posterior estimates of the lipid mass overlaid with the time series of lipid masses obtained using the estimated feeding activity on each day. In b)-f) disturbed days are distributed randomly, at the start of the trip, at the end of the trip, on days of low feeding activity and on days of high feeding activity, respectively. The shaded areas represent the uncertainty around the lipid mass predicted for each scenario. The horizontal dashed line represents a lipid mass of 0 kg.

Appendix S5. Testing the sensitivity of model results to selected dive metrics.

The feeding component of the model was structured with the aim of accommodating information from both horizontal movement and diving behavior, in order to characterize the feeding activity of an individual on a given day (Vacquié-Garcia et al. 2015). Ideally, proximate measures of feeding will be available in the future as data from accelerometers and jaw sensors are increasingly collected (e.g., Naito et al. 2013; Guinet et al. 2014). In the absence of such fine-scale indications of feeding attempts, we informed this model component using average features of an individual's diving pattern on a given day. We chose a data-driven approach (Appendix S1), where we selected the dive metric that best correlated with drift rate, under the assumption that successful feeding would lead to higher accumulation of lipid mass and thus higher buoyancy. This procedure supported the inclusion of dive metrics that previous studies have also identified as good proxies of feeding success in pinnipeds (e.g., Robinson et al. 2010; Viviant et al. 2014; Vacquié-Garcia et al. 2015). Selected dive metrics can also be interpreted from a functional perspective: a rapid ascent (and descent) rate maximizes the time in a foraging patch, and the number of dives might indicate that an area offers profitable food resources. In alternative to this data-driven approach, we could have decided to select, *a priori*, a dive metric that was mechanistically expected to represent successful feeding, such as the time spent at the bottom during a dive. Previous work has identified this metric as a good indicator of pinniped feeding activity (e.g., Austin et al. 2006; Gallon et al. 2013; Vacquié-Garcia et al. 2015), although some studies have also suggested that it is the behavior while at the bottom (particularly the engagement in rapid vertical excursions or wiggles) that is truly representative of prey pursuit (Kuhn et al. 2009; Gallon et al. 2013; Viviant et al. 2016). More generally, it is important to

explore the sensitivity of our results to the choice of the dive metrics that informed the feeding component.

To this purpose, we ran an alternative version of the model where we substituted median daily ascent rate (when positively buoyant) and total number of dives per day (when negatively buoyant) with the daily median time spent at the bottom during a dive (in both buoyancy conditions). We then compared the posterior estimates of feeding activity and lipid mass with the results from the final model, as well as the predicted effects of disturbance on sample individual 2005027.

The results of this comparison highlighted some fine-scale differences in the relative amount of feeding activity on any given day, although the overall pattern across the trip remained comparable (Fig. S6). The use of bottom time also resulted in a higher minimum value of feeding activity across the trip. While the accumulation of lipid mass over the trip remained unchanged (Fig. S6), this higher minimum had an influence on the predicted effects of disturbance: because a disturbed day was simulated by setting feeding activity to the minimum estimated for that individual, using bottom time in the feeding component resulted in the lipid mass at the end of the trip being, on average, 8% (SD = 5), 9% (SD = 6), 7% (SD = 6), 7% (SD = 5) and 10% (SD = 7) larger than in the final model for the scenarios with disturbed days distributed randomly, at the start of the trip, at the end of the trip, when feeding activity was lower and when feeding activity was higher, respectively (Fig. S7).

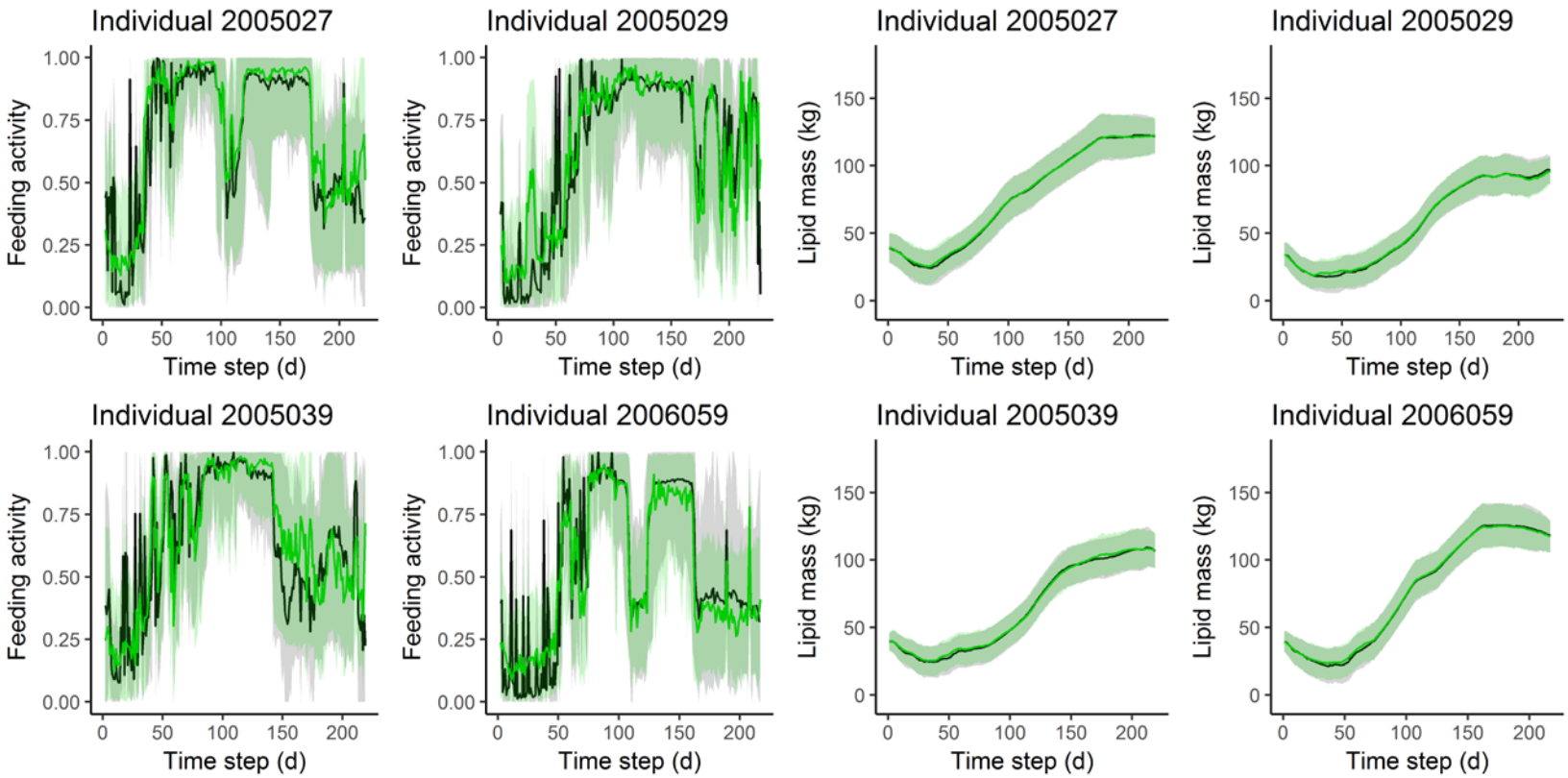

Figure S6. Comparison of the estimated feeding activity (on the left) and variation in lipid mass (on the right) given two alternative approaches to the selection of dive metrics for the feeding component, for four sample individuals. In black, the data-driven approach used in the final model, which led to include median ascent rate and total number of dives; in green, the alternative approach, where bottom time was used instead. The solid lines represent the median estimates, and the shaded bands the uncertainty around these estimates.

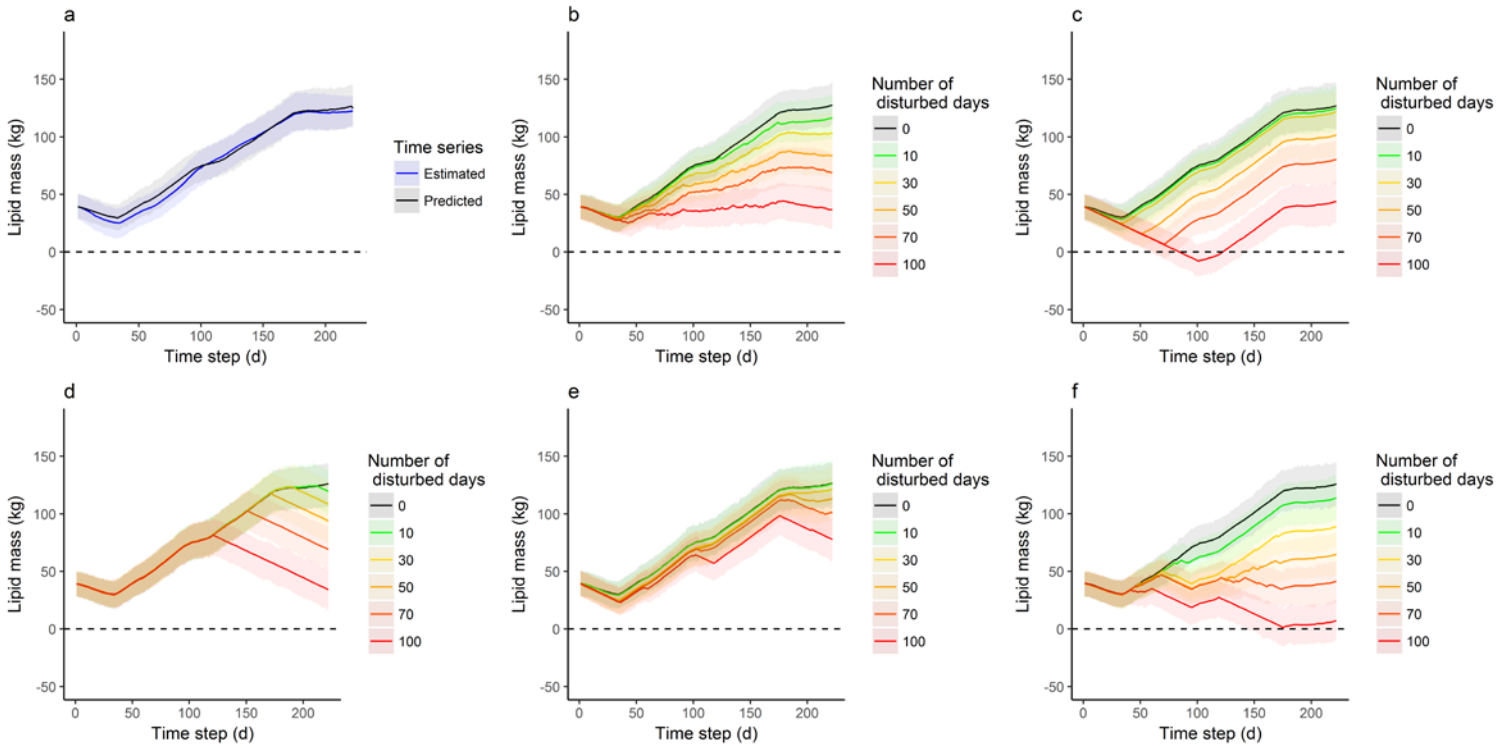

Figure S7. Simulated effects of an increased number of disturbed days on the lipid mass of individual 2005027, given the use of bottom time in the feeding component of the model. a) Posterior estimates of the lipid mass overlaid with the time series of lipid masses obtained using the estimated feeding activity on each day. In b)-f) disturbed days are distributed randomly, at the start of the trip, at the end of the trip, on days of low feeding activity and on days of high feeding activity, respectively. The shaded areas represent the uncertainty around the lipid mass predicted for each scenario. The horizontal dashed line represents a lipid mass of 0 kg.

References

Austin D, Don Bowen W, McMillan JI, Iverson SJ. 2006. Linking movement, diving, and habitat to foraging success in a large marine predator. Ecology 87:3095–3108. doi:10.1890/0012-9658(2006)87.

Bates D, Maechler M, Bolker B. 2012. lme4: Linear mixed-effects models using S4 classes. R package version 0.999999-0. Available at: http://cran.r-project.org/package=lme4.

Costa DP, Robinson PW, Arnould JPY, Harrison AL, Simmons SE, Hassrick JL, Hoskins AJ, Kirkman SP, Oosthuizen H, Villegas-Amtmann S, et al. 2010. Accuracy of ARGOS locations of pinnipeds at-sea estimated using fastloc GPS. PLoS One 5. doi:10.1371/journal.pone.0008677.

Gallon S, Bailleul F, Charrassin J-B, Guinet C, Bost C -a., Handrich Y, Hindell M. 2013. Identifying foraging events in deep diving southern elephant seals, Mirounga leonina, using acceleration data loggers. Deep Sea Res. Part II Top. Stud. Oceanogr. 88–89:14–22. doi:10.1016/j.dsr2.2012.09.002.

Guinet C, Vacquié-Garcia J, Picard B, Bessigneul G, Lebras Y, Dragon A, Viviant M, Arnould J, Bailleul F. 2014. Southern elephant seal foraging success in relation to temperature and light conditions: insight into prey distribution. Mar. Ecol. Prog. Ser. 499:285–301. doi:10.3354/meps10660.

Jonsen I, Flemming J, Myers RA. 2005. Robust state-space modeling of animal movement data. Ecology 86:2874–2880.

Kuhn CE, Crocker DE, Tremblay Y, Costa DP. 2009. Time to eat: measurements of feeding behaviour in a large marine predator, the northern elephant seal *Mirounga angustirostris*. J.

Anim. Ecol. 78:513–523. doi:10.1111/j.1365-2656.2008.01509.x.

McClintock BT, Russell DJF, Matthiopoulos J, King R. 2013. Combining individual animal movement and ancillary biotelemetry data to investigate population-level activity budgets. Ecology 94:838–849.

Naito Y, Costa DP, Adachi T, Robinson PW, Fowler M, Takahashi A. 2013. Unravelling the mysteries of a mesopelagic diet: A large apex predator specializes on small prey. Funct. Ecol. 27:710–717. doi:10.1111/1365-2435.12083.

New LF, Clark JS, Costa DP, Fleishman E, Hindell MA, Klanjšček T, Lusseau D, Kraus S, McMahon CR, Robinson PW, et al. 2014. Using short-term measures of behaviour to estimate long-term fitness of southern elephant seals. Mar. Ecol. Prog. Ser. 496:99–108. doi:10.3354/meps10547.

Robinson PW, Simmons SE, Crocker DE, Costa DP. 2010. Measurements of foraging success in a highly pelagic marine predator, the northern elephant seal. J. Anim. Ecol. 79:1146–1156. doi:10.1111/j.1365-2656.2010.01735.x.

Schick RS, New LF, Thomas L, Costa DP, Hindell MA, McMahon CR, Robinson PW, Simmons SE, Thums M, Harwood J, et al. 2013. Estimating resource acquisition and at-sea body condition of a marine predator. J. Anim. Ecol. 82:1300–1315. doi:10.1111/1365-2656.12102.

Vacquié-Garcia J, Guinet C, Dragon AC, Viviant M, Ksabi N El, Bailleul F. 2015. Predicting prey capture rates of southern elephant seals from track and dive parameters. Mar. Ecol. Prog. Ser. 541:265–277. doi:10.3354/meps11511.

Venables WN, Ripley BD. 2002. Modern Applied Statistics with S. Springer, New York.

Viviant M, Jeanniard-du-Dot T, Monestiez P, Authier M, Guinet C. 2016. Bottom time does not always predict prey encounter rate in Antarctic fur seals. Funct. Ecol. 30:1834–1844. doi:10.1111/1365-2435.12675.

Viviant M, Monestiez P, Guinet C. 2014. Can we predict foraging success in a marine predator from dive patterns only? Validation with prey capture attempt data. PLoS One 9:e88503. doi:10.1371/journal.pone.0088503.